Proto-TGO formation in TBC systems fabricated by spark plasma sintering

Mathieu Boidot [a], Serge Selezneff [a], Daniel Monceau [a,*], Djar Oquab [a], Claude Estournès [b]

[a] Institut Carnot CIRIMAT, ENSIACET 4, allée Emile Monso-BP 44362, 31030 Toulouse Cedex 4, France
[b] CNRS-CIRIMAT and PNF2-CNRS, 118 route de Narbonne, 31062 Toulouse Cedex 9, France

A B S T R A C T

Thermal barrier coatings (TBC) are commonly used in modern gas turbines for aeronautic and energy production applications. The conventional methods to fabricate such TBCs are EB-PVD or plasma spray deposition. Recently, the spark plasma sintering (SPS) technique was used to prepare new multilayered coatings. In this study, complete thermal barrier systems were fabricated on single crystal Ni-based superalloy (AM1®) substrate in a one-step SPS process. The lifetime of TBC systems is highly dependent on its ability to form during service a dense, continuous, slow-growing alumina layer (TGO) between an underlying bond coating and a ceramic top coat. In the present paper, we show that such kind of layer (called proto-TGO in the following) can be in situ formed during the SPS fabrication of TBC systems. This proto-TGO is continuous, dense and its nature has been determined using TEM-EDS-SAD and Raman spectroscopy. This amorphous oxide layer in the as-fabricated samples transforms to α-Al_2O_3 during thermal treatment under laboratory air at 1100 °C. Oxidation kinetics during annealing are in good agreement with the formation of a protective α-Al_2O_3 layer.

Keywords:
Thermal barrier coatings
Thermally grown oxide
Bond coating
Alumina
Spark plasma sintering

1. Introduction

The need to increase gas turbine efficiency has led to the development of thermal barrier systems during the past decades. The role of these multilayered systems is to decrease the surface temperature and thus the oxidation and corrosion rates of the superalloys constituting turbine blades and vanes. High-temperature oxidation and corrosion protection is achieved by the growth of a protective, continuous and dense oxide layer (generally alumina) on a MCrAl-RE (M = Ni and/or Co, RE = reactive element) overlay coating or on an aluminide diffusion coating [1,2]. Thermal protection relies on a ceramic insulating layer about 150 μm thick, typically yttria-stabilized zirconia (YSZ), deposited by air plasma spraying (APS) or electron beam physical vapor deposition (EBPVD) [2]. The fabrication process of a thermal barrier system with a diffusion aluminide bond coating is composed of a large number of steps including: several surface preparations, electrolytic Pt plating, high-temperature heat treatments under secondary vacuum, high-temperature vapor phase aluminization, heat treatment, pre-oxidation under low PO_2 atmosphere and deposition of the insulating ceramic (EB-PVD or APS). The number of parameters to control for the fabrication of these systems often limits the production of good quality laboratory samples.

The SPS technique has led to an important number of studies on the development of new materials (fully dense materials [3,4], functionally graded materials [5,6], difficult to sinter materials, nanosized grain ceramics [7–9] and composites…). However, only few authors have reported the possibility to coat parts with the SPS technique [10–12]. In recent papers [13–15], co-workers have demonstrated the ability of the SPS technique to fabricate MCrAlY, Pt-Al–modified MCrAlY overlay coatings, NiPtAl diffusion coatings and complete thermal barrier systems on nickel-based superalloy substrates. The purpose of this paper is to contribute to the understanding of the formation of an alumina layer during SPS fabrication of a complete thermal barrier system.

2. Experimental procedure

2.1. Materials

The standard stack-up of materials used for SPS complete TBC systems fabrication is composed of the following materials and is described in Fig. 1

1/ a 24 mm diameter Ni-based superalloy substrate (AM1®), the composition and description of which is reported elsewhere [16]. Samples were ground with European grade 600 SiC paper before being oxidized in air for 1 h at 1100 °C. After air-quenching, the top face of the coupons was ground again with 600 SiC paper to remove the oxide layer. This procedure leaves a 1 μm oxide on all the parts of the substrates except the one to coat. This oxide acts as a carbon diffusion barrier during processing [15];
2/ a Pt-modified nickel aluminide bond coating prepared from Pt (2 or 5 μm thick) and Al foils (2 μm thick) (Goodfellow Corp.). In ref. [15], the possibility to dope the bond coating with reactive elements (Hf, Y) and Si is also reported.

* Corresponding author. CIRIMAT-ENSIACET 4, allée Emile Monso-BP 44362, 31030 Toulouse cedex 4, France. Tel.: +33 5 34 32 34 22; fax: +33 5 34 32 34 98.
E-mail address: daniel.monceau@ensiacet.fr (D. Monceau).

doi:10.1016/j.surfcoat.2010.09.042

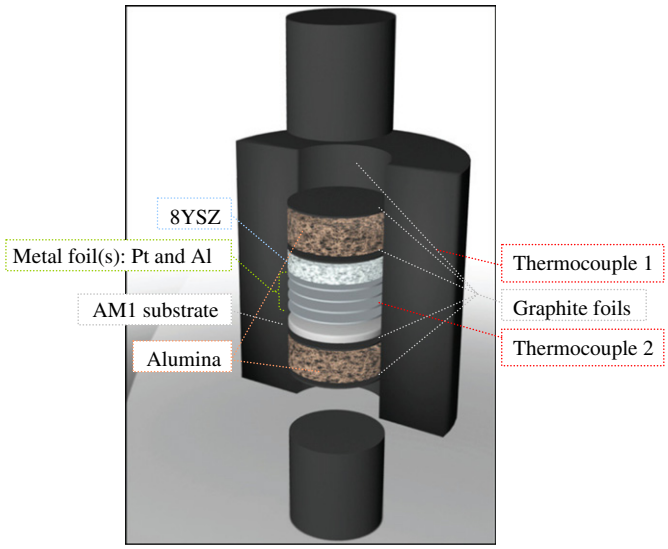

Fig. 1. Standard stack and thermocouples location for temperature monitoring during the spark plasma sintering process.

3/ a partially yttria-stabilized zirconia (YSZ) ceramic top coat composed of commercial fine grain (50–200 nm, 6 ± 2 m^2/g) 8 or 10 mol% YSZ (Tosoh Corp.).

2.2. Spark plasma sintering

A Dr Sinter 2080 (SPS Syntex Inc., Japan) SPS apparatus was used for fabrication of the thermal barrier systems. A standard 12/2 on/off 3.3 ms pulse pattern was used. Graphite punches and die were used. The temperature was monitored by a K-type thermocouple placed in a 3-mm-deep hole at the surface of the die (thermocouple 1) and the actual temperature of the sample was measured at the contact point with a second thermocouple (2) as shown in Fig. 1.

Depending on the temperature set point, a difference up to 150 °C was measured between the two thermocouples (the latter being hotter than the former). To enhance reproducibility, two electric barriers of alumina powders were placed in the graphite die on each part of the sample. These alumina barriers deflect the lines of electric current in the conducting graphite die (rather than passing through the sample) and then prevent the system from local overheating during processing as it is now heated by the die.

The thermal cycle during SPS consisted of heating the sample from room temperature to 1100 °C at 100 °C/min, and it was maintained at this temperature for 1 to 30 min. An additional dwell at 700 °C is added, before the 1100 °C dwell, when aluminum foil is used. The cooling is either unmonitored or at 20 °C/min. The pressure pattern begins with an initial dwell of 2 min at 0.2 MPa followed by an increase in 1 min to the desired pressure (16, 25 or 50 MPa). Then the pressure is held until the end of the thermal cycle and then relaxed in 1 min. A following heat treatment has been performed in air at 1100 °C for 5 or 10 h on sample D (Table 1).

Table 1 gives all needed details on the assemblies, SPS and heat treatments of the different samples.

2.3. Characterization

Microstructural investigations were performed with a LEO 435 VP SEM equipped with a PGT EDX analyzer and with a JEOL Jem 2010 TEM. The samples were previously cross-sectioned, mounted in a resin and ground with SiC paper from grade 600 to 2400, and then polished up to 1 μm diamond paste. For composition profiles, analysis zones were 1*200 μm boxes parallel to the surface of the samples. The composition given is a quantitative mean value for each box. The calculations were made using real standards.

Cr^{3+} fluorescence spectra were recorded with a Raman spectrophotometer Jobin Yvon-Spex Horiba T64000 with a Raman laser wavelength of 514.532 nm.

Table 1
References of the fabricated samples. BC*: 5 μm Pt foil + 2 μm Al foil. [1]: secondary air vacuum in the SPS chamber.

Sample Name	Assembly	SPS			Heat treatment	
		t (min)	T (°C)	P (MPa)	t (h)	T (°C)
A[1]	AM1/Pt 2 μm/TZ10Y	10	1100	16		
B[1]	AM1/BC*/TZ8Y	10	700	16		
		10	1100			
C[1]	AM1/BC*/TZ8Y	10	700	25		
		10	1100			
D[1]	AM1/BC*/TZ8Y	10	700	50		
		10	1100			
D1[1]	AM1/BC*/TZ8Y	10	700	50	5	1100
		10	1100			
D2[1]	AM1/BC*/TZ8Y	10	700	50	10	1100
		10	1100			
D3[1]	AM1/BC*/TZ8Y	10	700	50	15	1100
		10	1100			

3. Observations

SPS fabricated TBCs exhibit a dense, homogeneous and default-free bond coating (BC; Fig. 2a). Fig. 2b shows that the bond coating is dense and adherent after SPS. It contains no Kirkendall voids and former interfaces between the foils and with the superalloy substrate are invisible. The ceramic top coat is adherent, fracture-free and its volume porosity has been measured by image analysis. The value of $18 \pm 3\%$ is achieved by selecting the appropriate SPS parameters depending on the YSZ grain size. A thin oxide layer, continuous and adherent, has grown during the SPS fabrication process. The TEM micrograph reported in Fig. 2c confirms that this layer is homogeneous, amorphous and between 200 and 300 nm in thickness. We can also note that some YSZ grains are trapped in this layer.

On the composition profiles given in Fig. 2d we can see clearly the uphill diffusion of aluminum in the bond coating. Indeed, this sample (A) did not contain an Al foil, i.e. Al is diffusing from the substrate to the surface because of its activity gradient due to the Pt effect [20]. Reporting the composition of the different layers on a NiPtAl ternary phase diagram shows that the bond coating is composed of the α-$NiPt_2Al$ [17,18] and γ′- Ni_3Al phases Fig. 2b.

In order to transform both the α-$NiPt_2Al$ phase into γ'-Ni_3Al and the proto-TGO into α-Al_2O_3, we have performed a thermal treatment at 1100 °C under air for several durations (Fig. 3). Due to diffusion phenomena, the proto-TGO as well as bond coating have grown in thickness and phase transformations have occurred. After 5 h, there are still few grains of α-$NiPt_2Al$ (Fig. 3a) near the TGO region whereas α has completely transformed into γ′ after 10 h of annealing (Fig. 3b). After thermal treatment, the TGO has been identified by fluorescence spectroscopy as α-Al_2O_3 (Cr^{3+} fluorescence peaks in α-Al_2O_3 at 14360 cm^{-1} and 14396 cm^{-1}).

4. Discussion

4.1. Formation of the proto-TGO

The formation of an alumina TGO layer in a conventional EB-PVD thermal barrier system is achieved by a pre-oxidation treatment before EB-PVD top coat deposition and by growth during the EB-PVD process. In the case of a SPS fabricated thermal barrier system, there is no pre-oxidation treatment before top coat deposition, as it is a one-

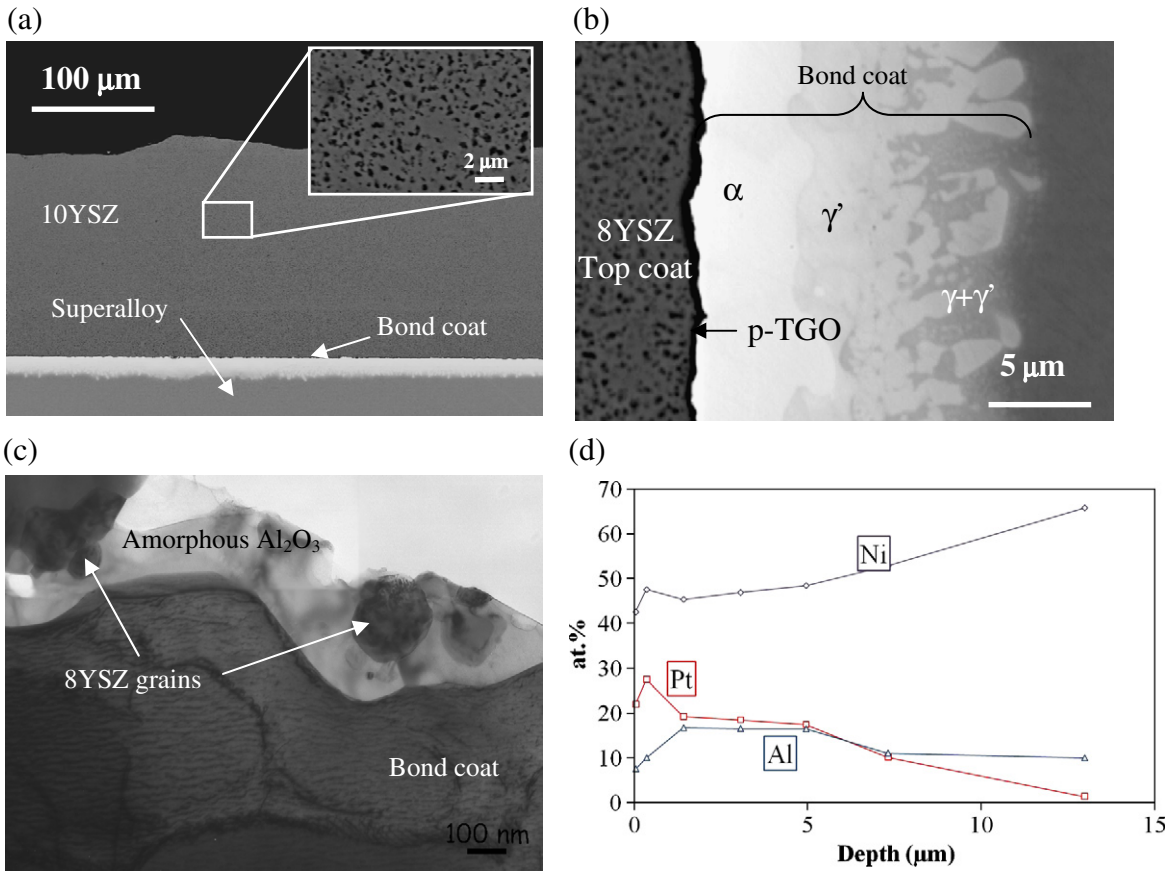

Fig. 2. (a) Microstructure of an SPS-fabricated TBC (sample A). (b) microstructure with phase labeling of a bond coating made at 1100 °C during 10 min with 50 MPa during SPS. (Sample D) (c) TEM micrograph showing an alumina layer (proto-TGO) with entrapped ZrO_2 grains between BC and TC (sample A) and (d) composition profile with uphill diffusion of Al through the bond coating during SPS process (sample A).

step process. Nevertheless, an amorphous alumina layer called proto-TGO has grown between bond coating and top coat in SPS processed samples. The name proto-TGO refers to the fact that this layer has grown during the fabrication process and that it is seen as a precursor for its final form, α-Al_2O_3, which will form during subsequent annealing or during use at high temperature.

In order to understand the formation of this proto-TGO during SPS process, the origin of its individual components (e.g. Al and O) must be determined. There are two sources of Al in the system: Al from the added metallic foil and Al from the superalloy substrate. As Al_2O_3 proto-TGO has been observed on sample A (without Al foil addition), we know that Al is able to diffuse from the superalloy to the proto-TGO in the time lapse of the SPS experiment (10 min at high temperature). This phenomenon is clearly shown in Fig. 2d, where the aluminum concentration is close to 8 at.% at a few nanometers under the proto-TGO. The minimum diffusion coefficient of Al for a 2 µm migration in Pt, in 10 min at 1100 °C, is about 10^{-15} m^2/s. This value is close to the one of the diffusion coefficient of Al in Ni given by Watanabe et al. [22,23]. Then, simple diffusion could be sufficient to explain the presence of Al below the TGO. Nevertheless, two

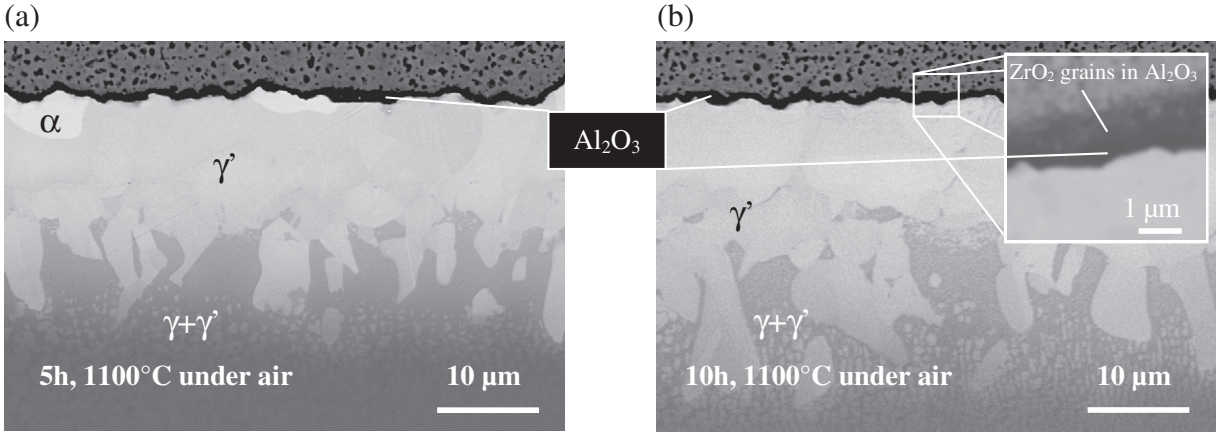

Fig. 3. Cross-section SEM-BSE micrographs of SPS fabricated TBCs (10 min 1100 °C, 16 MPa) after thermal treatment (a) 5 h (sample D1) and (b) 10 h (sample D2) at 1100 °C under air.

additional driving forces are available and can enhance the transport of Al towards the TGO. The first one is the Al activity gradient due to the effect of Pt [20,21]. The second one is the electric field in the SPS which could lead to electromigration [19] as the electric current always flows in the same direction in the SPS apparatus.

Determining the origin of oxygen in the proto-TGO is more difficult as it has several possible sources. It could come either from the gas contained in the pores of the non-compacted initial powder, from the atmosphere of the SPS chamber (dynamic vacuum of air) or from the oxygen contained in yttria-stabilized zirconia. It can also be a combination of these phenomena.

Xue et al. [24] have demonstrated that platinum reacts with zirconia to form metallic zirconium which diffuses in platinum at 1300 °C. Assuming that this phenomenon also occurs at 1100 °C, the amount of oxygen released by zirconia, according to ref. [24], would be too small to be responsible for the formation of the whole proto-TGO observed. Besides, if Al_2O_3 is formed from the reduction of ZrO_2, this would lead to Zr formation and diffusion in the bond coating which was searched for and not observed by EPMA.

The other hypothesis is the oxygen trapped between YSZ grains. The comparison of the amount of oxygen contained in the air trapped in the porosity of the yttria-stabilized zirconia ($n_{O_{porosity}}$) to its amount in the alumina proto-TGO layer ($n_{O_{p\text{-}TGO}}$) is given by the following ratio:

$$\frac{n_{O_{porosity}}}{n_{O_{p-TGO}}} = \frac{2}{3}\frac{P_{O_2} \times e_{YSZ} \times p \times M_{Al_2O_3}}{RT \times \rho_{Al_2O_3} \times e_{Al_2O_3}} \quad (1)$$

where $P_{O_2}$is the O_2 pressure in the SPS chamber at room temperature; e_{YSZ} and p are TBC thickness and porosity (between 0 and 1); ρ_{Al_2O3} and $M_{Al_2O_3}$ are the density and the molecular weight of amorphous alumina and where the gas contained in the porosity of the top coat is supposed to be perfect.

Calculation shows that for a range of porosity between 10 and 50 vol.% the ratio $\frac{n_{O_{porosity}}}{n_{O_{p-TGO}}}$ is always lower than 7.10^{-12} so the amount of oxygen contained in the porosity of the YSZ layer is far too small to be responsible for the proto-TGO formation.

The chamber volume is filled with low-pressure air (5 Pa) corresponding to $P_{O2} = 1$ Pa which is far higher than the O_2 partial pressure required to form Al_2O_3 at 1100 °C (about 10^{-30} atm). As the SPS experiment is carried out in dynamic vacuum, there is a constant flow of air in the chamber through leakages. The O_2 partial pressure near the sample is governed on the one hand by the equilibrium between C (graphite die) and O_2, CO, CO_2 gases at 1100 °C and by the flow of gas due to pumping on the other hand. Equilibrium calculations in a closed system initially composed of solid carbon and air at 5 Pa have been performed with HSC chemistry software. Final P_{O2} obtained at 1100 °C is 10^{-18} Pa. On the contrary, if the reaction rate between C (graphite die) and O_2 is negligible before the flow of gas into the chamber, it can be assessed that P_{O2} lies between 10^{-18} Pa and 1 Pa. At 1100 °C, the reaction between Al and O_2 at this P_{O2} easily forms Al_2O_3.

4.2. High-temperature oxidation

We have measured the oxide scale (TGO) thickness after SPS and after several oxidation durations (5, 10 and 15 h) at 1100 °C. The results are reported in Fig. 4. For oxidation durations of 5 h or more, the oxide thickness increases linearly with square root of time which indicates that TGO growth is a diffusion-controlled growth mechanism. The initial oxidation kinetics appears to be faster. Using these data, the local parabolic constant (k_p in mg²/cm⁴/s) of the oxidation kinetics can be calculated using [25]:

$$K_p = F^2\left(e_2^2 - e_1^2\right) / (t_2 - t_1) \quad (2)$$

where e_2 and e_1 are the oxide scale thicknesses at time t_2 and t_1, and where F is a factor allowing the conversion from the scale thickness to the oxygen mass gain by unit surface area ($F = 0.185$ mg/cm² for a 1 μm thick α-Al_2O_3 oxide layer). The values show a large decrease of the oxidation parabolic coefficient with time (Fig. 4). It can be interpreted as the succession of two parabolic regimes which are due to the formation of amorphous alumina proto-TGO during SPS processing and then to the growth of the α-alumina TGO layer after transformation of the proto-TGO. This is supported by the fact that the final parabolic constant ($4.2.10^{-7}$ mg²/cm⁴/s) is close to the known value for alumina growth on β-NiAl ($1.5.10^{-7}$ mg²/cm⁴/s) [26], and the first parabolic constant corresponding to the growth in the SPS ($6.6.10^{-6}$ mg²/cm⁴/s) is close of the known values for the growth of transition aluminas at 1100 °C (7.10^{-6} mg²/cm⁴/s for a theta-alumina at 1100 °C) [26].

5. Conclusion

The use of SPS as a fast development tool for new thermal barrier systems has been efficient in recent years. This process has shown great reproducibility so far and is versatile and easy to use compared to the important number of stages in the fabrication of a state-of-the-art EBPVD or APS TBC. The presence of an alumina proto-TGO on

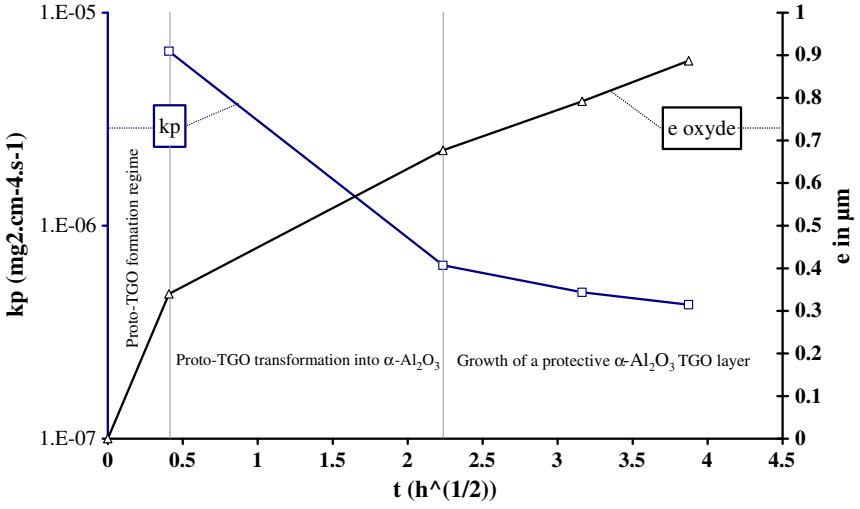

Fig. 4. Thickness of TGO (e) and calculated parabolic constant (k_p) after SPS (sample D) and after several oxidation durations: 5 h (D1), 10 h (D2) and 15 h (D3), at 1100 °C.

fabricated samples has been observed and assessments of its origin are summarized below:

- Aluminum present in the proto-TGO diffuses from the superalloy during SPS experiment (10 min at 1100 °C) across 2 μm of pure platinum;
- The SPS chamber if filled with flowing air at 5 Pa. Local equilibrium between C, O_2, CO and CO_2 do not prevent oxidation of the sample.
- Amorphous alumina proto-TGO is formed during SPS process and transforms into α-Al_2O_3 after heat treatment without leading to crack or delamination of the TBC system in isothermal annealing at 1100 °C, or thermal cycling at 1100 °C [15].
- Oxidation kinetics calculations show that the proto-TGO formed during SPS processing has a similar growth rate as a θ-alumina scale. During isothermal oxidation, this proto-TGO rapidly transforms into a slow-growing α-alumina layer.

Acknowledgments

Authors kindly thank Snecma-SAFRAN and DGA for financial support of this work. We are also grateful to Mrs. M.C. Lafont for TEM analysis.

References

[1] A. Rabiei, A.G. Evans, Acta Mater. 48 (2000) 3963.
[2] M.J. Stiger, N.M. Yanar, M.G. Topping, F.S. Pettit, G.H. Meier.
[3] Q. He, C. Jia, J. Meng, Mater. Sci. Eng. A 428 (2006) 314.
[4] G. Xie, D.V. Louzguine-Luzgin, H. Kimura, A. Inoue, Appl. Phys. Lett. 90 (2007).
[5] Z. Shen, M. Johnsson, M. Nygren, J. Eur. Ceram. Soc. 23 (2003) 1061.
[6] L. Yongming, P. Wei, L. Shuqin, W. Ruigang, L. Jianqiang, Mater. Sci. Eng., A 345 (2003) 99.
[7] X. Xu, T. Nishimura, N. Hirosaki, R.J. Xie, Y. Yamamoto, Adv. Si-Based Ceram. Compos. 287 (2005) 166.
[8] L. Gao, Z.J. Shen, H. Miyamoto, M. Nygren, J. Am. Ceram. Soc. 82 (1999) 1061.
[9] W.-W. Wu, G.-J. Zhang, Y.-M. Kan, P.-L. Wang, K. Vanmeensel, J. Vleugels, O. Van der Biest, Scr. Mater. 57 (2007) 317.
[10] L.G. Yu, K.A. Khor, H. Li, K.C. Pay, T.H. Yip, P. Cheang, Surf. Coat. Technol. 182 (2004) 308.
[11] K.A. Khor, X.J. Chen, S.H. Chan, L.G. Yu, Mater. Sci. Eng., A 366 (2004) 120.
[12] K.A. Khor, L.G. Yu, S.H. Chan, X.J. Chen, J. Eur. Ceram. Soc. 23 (2003) 1855.
[13] D. Oquab, C. Estournes, D. Monceau, Adv. Eng. Mater. 9 (2007) 413.
[14] D. Oquab, D. Monceau, Y. Thébault, C. Estournes, Mater. Sci. Forum 595–598 (2008) 143.
[15] D. Monceau, D. Oquab, C. Estournes, M. Boidot, S. Selezneff, Y. Thebault, Y. Cadoret, Surf. Coat. Technol. 204 (2009) 771.
[16] P. Caron, T. Khan, Aerosp. Sci. Technol. 3 (1999) 513.
[17] S. Hayashi, S.I. Ford, D.J. Young, D.J. Sordelet, M.F. Besser, B. Gleeson, Acta Mater. 53 (2005) 3319.
[18] H. Meininger, M. Ellner, J. Alloy. Comp. 353 (2003) 207.
[19] P.S. Ho, T. Kwok, Rep. Prog. Phys. 52 (1989) 301.
[20] B. Gleeson, W. Wang, S. Hayashi, D. Sordelet, Mater. Sci. Forum 461–464 (2004) 213.
[21] S. Hayashi, W. Wang, D.J. Sordelet, B. Gleeson, Metall. Mater. Trans. A Phys. Metall. Mater. Sci. 36A (2005) 1769.
[22] M. Watanabe, Z. Horita, D.J. Smith, M.R. McCarney, T. Sano, M. Nemoto, Acta Metall. Mater. 42 (1994) 3381.
[23] M. Watanabe, Z. Horita, D.J. Smith, M.R. McCarney, T. Sano, M. Nemoto, Acta Metall. Mater. 42 (1994) 3389.
[24] J. Xue, R. Dieckmann, Solid State Ionics 53–6 (1992) 209.
[25] D. Monceau, B. Pieraggi, Oxid. Met. 50 (1998) 477.
[26] M.W. Brumm, H.J. Grabke, Corros. Sci. 33 (1992) 1677.